CERN – EUROPEAN ORGANIZATION FOR NUCLEAR RESEARCH

CLIC – Note – 1024

CONCEPTUAL DESIGN OF THE POST-PETS INSTRUMENTATION LINE FOR CLIC

M. Olvegård and V. Ziemann
Uppsala University, Sweden

Abstract

We propose a method to measure the time-resolved momentum distribution and beam size at the end of the decelerator in the drive beam complex of the Compact Linear Collider, CLIC. Conventional diagnostic methods are hampered by the very high beam power and large energy spread of the drive beam after up to 90% of its kinetic energy is converted into microwave power. Our method is based on sweeping the beam in a circular pattern to determine the momentum distribution and recording the beam size on a screen using optical transition radiation. We present an algorithm to extract the time-resolved momentum distribution. Furthermore, qualitative information about the beam size along the pulse train can be extracted from the image left on a screen by sweeping the beam linearly. We present simulation results that allow us to estimate the applicability.

Geneva, Switzerland
2013

Conceptual design of the post-PETS instrumentation line for CLIC

M. Olvegård and V. Ziemann

Uppsala University, P.O. Box 516, SE-751 20, Sweden

Abstract

We propose a method to measure the time-resolved momentum distribution and beam size at the end of the decelerator in the drive beam complex of the Compact Linear Collider, CLIC. Conventional diagnostic methods are hampered by the very high beam power and large energy spread of the drive beam after up to 90% of its kinetic energy is converted into microwave power. Our method is based on sweeping the beam in a circular pattern to determine the momentum distribution and recording the beam size on a screen using optical transition radiation. We present an algorithm to extract the time-resolved momentum distribution. Furthermore, qualitative information about the beam size along the pulse train can be extracted from the image left on a screen by sweeping the beam linearly. We present simulation results that allow us to estimate the applicability.

1. Introduction

In the CLIC drive beam decelerator, up to 90% of the incoming beam power will be extracted from the drive beam [1, 2]. The deceleration leaves the beam with the energy distribution depicted in Fig. 1, with a high energy transient at the head of the bunch train, shown in Fig. 1(a), reaching all the way to the initial energy. The majority of the bunches, in the steady state of the pulse, lose 90% of their energy. The resulting energy distribution, shown in Fig. 1(b) has a peak around the minimum energy with a long tail extending into higher energies . The momentum distribution in the beam needs to be monitored for an optimum set-up of the decelerator. In the test beam line at the CLIC test facility, CTF3, the drive beam decelerator is being experimentally studied in small-scale. The analysis of the beam profile diagnostics in TBL in Refs. [3] and [4] has shown that segmented beam dumps, currently used for time-resolved spectrometry in TBL, are not suitable for the CLIC decelerators due to the high beam power. On the other hand, OTR screens have a good chance of surviving the high intensity. We therefore intend to base the time-resolved measurements of transverse and energy profile in the CLIC decelerator on OTR screens. The general layout envisioned for the diagnostics is to have two scanning kicker magnets sitting in the same place in the beamline; One kicking in the vertical direction and the other in the horizontal direction, similarly to the dilution kickers in the LHC dump line, which forms the figure “e” of the beam on a screen [5]. We assume that the kickers can be excited in a cycle corresponding to the 240 ns drive beam duration and with a rise of the magnetic field that provides a kick from zero to a few milliradian in the same time range. Furthermore, we assume that the magnet excitation can be made in a way that the horizontal kicker is driven by a cosine wave while the vertical is driven by a sine wave, thus making it possible to form a Lissajous figure of the beam on the screen. Forming the sweep into a circle allows us to analyze the momentum distribution along the beam pulse. A linear sweep in one direction at a time gives information about the transverse beam distribution along the pulse.

We will begin with discussing spectrometry for large momentum spread beams. Then, we will turn to the particular measurement set-up proposed for the post-PETS line. There, we will first predict what will be seen on the screen for a given beam distribution in time and momentum when the circular sweep is applied. Finally, we will show examples of the measurement and of the analysis.

2. Spectrometry for beams with large momentum spread

Spectrometry is a common way of measuring the momentum content of a particle beam. Under normal circumstances the dispersion function is used to calculate the momentum spread in a beam, though strictly speaking, the

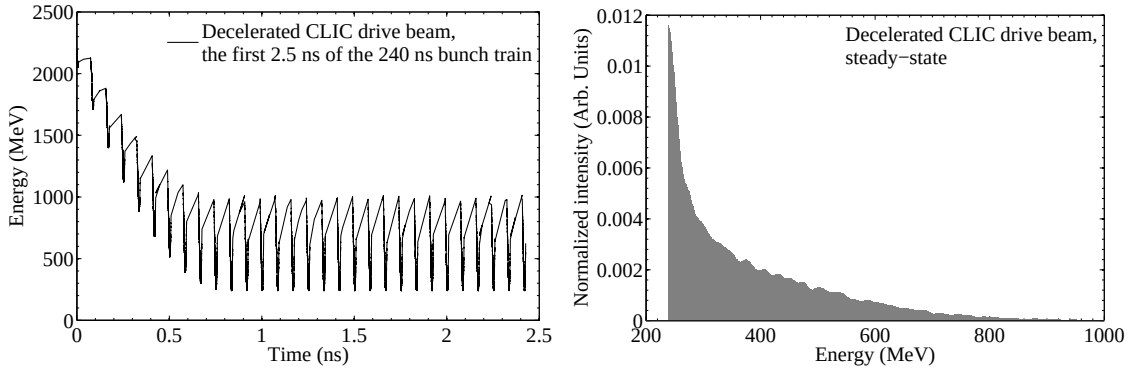

(a) Energy transient (b) Histogram of the steady-state

Figure 1: The energy distribution in the decelerated CLIC drive beam, simulated with PLACET [6]. The high energy transient (a) extends all the way up to the initial energy of 2.4 GeV and is followed by a 240 ns long steady-state. The transient contains very few particles compare to the rest of the bunch train and the histogram to the right (b) shows only the energy content of the steady-state.

dispersion function is only valid for small momentum spread. For large spread it leads to a misinterpretation of the spectrometer measurements, in the worst case to unphysical results, such as negative momenta. In such cases, we need to consider momentum deviation in a more stringent manner. For this purpose, we assume a momentum distribution $\psi(\delta)$, that enters a spectrometer magnet, deflecting in the horizontal plane. Here, we use the parametrization $\delta = (p - p_0)/p_0$ for the momentum where p_0 is the reference momentum. The distribution is mapped onto a screen or equivalent in a spectrometer line at a distance L from the deflection center, as in the sketch in Fig. 2.

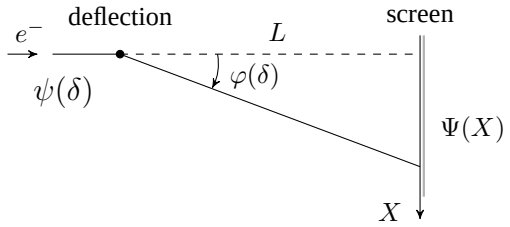

Figure 2: Sketch of a horizontal deflection onto a screen, defining the variables used in the equations.

A particle with momentum δ will have a final position on the screen $X \approx L\varphi(\delta)$ where $\varphi(\delta)$ is the deflection angle. Let $D_0 = L\varphi_0$ with the index 0 referring to the position on the screen that is hit by a particle with the reference momentum. Incidentally, D_0 coincides with the dispersion generated by the dipole, and we get

$$X = \frac{D_0}{1+\delta}\,. \tag{1}$$

When the momentum spread is small, i.e. when $\delta << 1$, we can expand the expression in powers of δ and obtain the linear approximation $X \approx D_0(1-\delta)$. In our case, however, the assumption is not valid and the approximation can not be made. Instead, we use Equation (1) to determine the particle density on the screen by integrating over all initial momenta through

$$\Psi(X) = \int \psi(\delta)\,\delta_D\left(X - \frac{D_0}{1+\delta}\right) d\delta \tag{2}$$

where δ_D denotes the Dirac delta function. We start with the integration over δ and use the relation

$$\delta_D(g(u)) = \sum_i \frac{\delta_D(u-u_i)}{|g'(u_i)|} \quad \Longrightarrow \quad \int f(u)\delta_D(g(u))dx = \sum_i \frac{f(u_i)}{|g'(u_i)|} \tag{3}$$

where u_i are the zeros of $g(u)$. In our case, $g(\delta) = X - D_0/(1+\delta)$ with one zero at $\delta = (D_0 - X)/X$ and with $g'(\delta_0) = X^2/D_0$. The particle distribution on the screen is then given by

$$\Psi(X) = \frac{D_0}{X^2}\,\psi\left(\frac{D_0 - X}{X}\right) \tag{4}$$

where X is the coordinate on the screen in the plane of deflection and D_0 is the reference dispersion, e.g. for the position of the momentum peak.

Normally, we are interested in deducing the moment profile from the geometric profile on a spectrometer screen. To do so we need the inverted transformation. It is calculated in the same way and reads

$$\psi(\delta) = \frac{D_0}{(1+\delta)^2}\,\Psi\left(\frac{D_0}{1+\delta}\right). \tag{5}$$

As an example we look at a Gaussian momentum distribution of rms width Δ,

$$\psi(\delta) = \frac{1}{\sqrt{2\pi}\Delta} e^{-\delta^2/2\Delta^2}. \tag{6}$$

Through the operation in Eq. (4) we obtain the particle distribution on the screen

$$\Psi(X) = \frac{1}{\sqrt{2\pi}\Delta}\frac{D_0}{X^2}\exp\left(-\frac{(D_0 - X)^2}{2\Delta^2 X^2}\right). \tag{7}$$

We see from Eq. (7) that the low energy tail becomes more pronounced on the screen as the spread Δ grows larger. Figure 3 shows an example with $D_0 = 0.3$ m and a Gaussian momentum distribution with rms spread varied between 5% and 15%. We note that the asymmetry is hardly visible for the smallest spread while quite apparent for the largest spread.

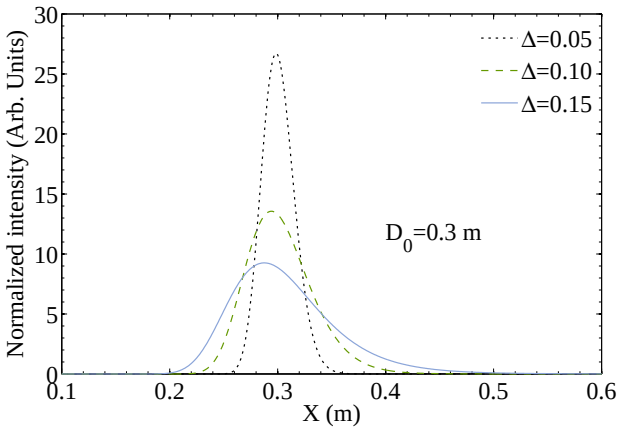

Figure 3: A Gaussian momentum profile becomes asymmetric when projected onto a spectrometer screen. The asymmetry grows with increasing momentum spread Δ.

If, instead of using Eq. (5) to analyze such a spectrometer distribution, we assume that $\delta << 1$ and use the linear approximation $X \approx D_0(1-\delta)$, we commit an error. In order to illustrate this error we use the profile from Fig. 3 corresponding to the largest momentum spread $\Delta = 0.15$. We apply the inverse transformation, but based on the assumption that δ is small. The resulting distribution is presented in Fig. 4 together with the correct Gaussian distribution. The asymmetry that appeared on the screen translates into a distorted momentum profile where the peak has shifted 4.1% towards higher momentum. The rms width becomes 45% larger than the original while the fwhm width is 7.5% smaller than the input value.

The situation becomes even more critical if we consider the energy distribution at the end of a CLIC drive beam decelerator. The distribution is peaked at 240 MeV but has a long tail that extends all the way up to the maximum

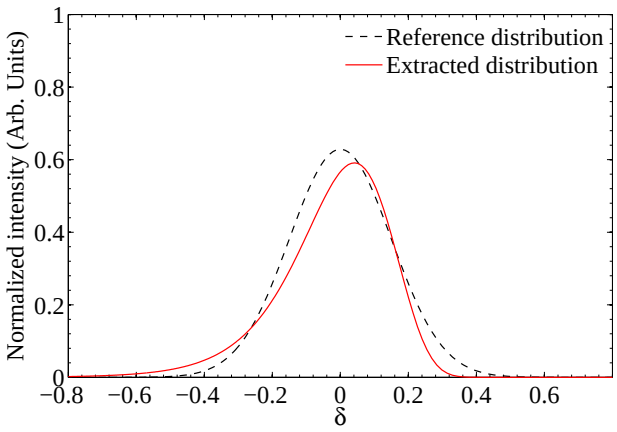

Figure 4: The extracted momentum distribution compared to the reference distribution, when the extracted profile has been calculated using the approximation $\delta \approx (D_0 - X)/D_0$ instead of the correct relation $\delta = (D_0 - X)/X$.

energy of 2.4 GeV. If $p_0 = 240$ MeV, δ will reach as high as 10, with the vast majority of the particles within the steady-state, with $\delta < 4$. This distribution, projected on a screen with $D_0 = 0.3$ m, is shown in Fig. 5. Again, we use the linear approximation $X = D_0(1 - \delta)$ to extract the momentum distribution from the screen and obtain the profile shown in Figure 6. As a reference, we show also the input momentum distribution, the presence of which highlights that the distribution extracted incorrectly is a severely distorted version of the real. The initial momentum distribution is recovered if Equation (5) is employed for the analysis of the spectrometer profile.

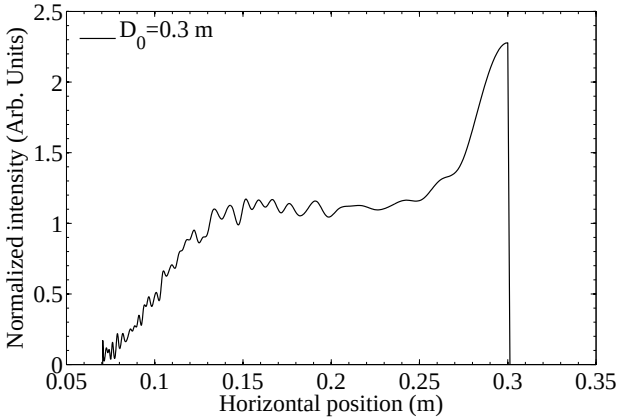

Figure 5: The beam distribution at the end of a CLIC drive beam decelerator (see Fig. 1(b)) projected on a screen, with $D_0 = 0.3$ m for $E_0 = 240$ MeV. The sharp edge corresponds to the beam particles that have experienced maximum deceleration.

Now that we have established the correct way of analyzing spectrometer profiles for large momentum spreads we turn to discuss a method to obtain time-resolved information about the beam pulse.

3. Time-resolved spectrometry

In order to establish a way of extracting time-resolved information from the spectrometer measurement we first look at how a particle distribution transforms when projected onto a screen. We use the variables defined in Fig. 2 and introduce a rotating effective magnetic field vector so that a particle with momentum δ hits the screen at the coordinates

$$X = \frac{L\varphi_0 \cos(2\pi\tau)}{1+\delta}, \qquad Y = \frac{L\varphi_0 \sin(2\pi\tau)}{1+\delta} \tag{8}$$

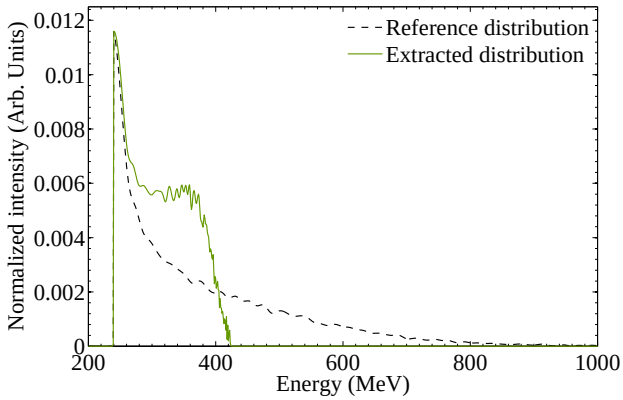

Figure 6: The dashed line is the reference energy distribution and the solid line is the distribution extracted from a spectrometer measurement in Fig. 5 using the approximation of linear dispersion.

with $\tau = t/T$ where T is the period of the magnetic cycle and $0 < \tau < 1$. Note that the magnet sprays the beam on a sector of a circle on the screen. The cycle time T has to be matched to the bunch train duration in order to avoid overlap of the tail with the head of the beam.

Let further $\psi(\tau, \delta)$ be the initial particle density distributed over time and momentum. We ignore for now the emittance and obtain the transverse particle distribution on the screen $\Psi(X, Y)$ by integrating over time and momentum through

$$\Psi(X,Y) = \iint \psi(\tau,\delta)\,\delta_D\left(X - \frac{L\varphi_0\cos(2\pi\tau)}{1+\delta}\right)\delta_D\left(Y - \frac{L\varphi_0\sin(2\pi\tau)}{1+\delta}\right)d\tau d\delta\,. \tag{9}$$

This is an integral over two dimensions and we use the Jacobi determinant to transform the integration variables from (τ, δ) to (X, Y). It is defined through

$$\det(J) = \begin{vmatrix} \partial X/\partial\tau & \partial X/\partial\delta \\ \partial Y/\partial\tau & \partial Y/\partial\delta \end{vmatrix} \tag{10}$$

With the Jacobi determinant the integral in Eq. (9) transforms as

$$\Psi(X,Y) = \iint \psi(\tau,\delta)\,\delta_D\left(\tau - \frac{1}{2\pi}\arctan\left(\frac{X}{Y}\right)\right)\delta_D\left(\delta + 1 - \frac{l\varphi_0}{\sqrt{X^2+Y^2}}\right)\frac{1}{|\det(J)|}\,d\tau d\delta \tag{11}$$

where we use the fact that

$$X^2 + Y^2 = \left(\frac{L\phi_0}{1+\delta}\right)^2 \qquad \text{and} \qquad \frac{Y}{X} = \tan(2\pi\tau)\,. \tag{12}$$

The matrix elements for the determinant are easily derived through differentiation with the result

$$\frac{\partial X}{\partial\tau} = -2\pi\frac{L\phi_0}{1+\delta}\sin(2\pi\tau) = -2\pi Y \qquad \frac{\partial X}{\partial\delta} = -\frac{L\phi_0}{(1+\delta)^2}\cos(2\pi\tau) = -\frac{X}{1+\delta}$$

$$\frac{\partial Y}{\partial t} = 2\pi\frac{L\phi_0}{1+\delta}\cos(2\pi t) = 2\pi X \qquad \frac{\partial Y}{\partial\delta} = -\frac{L\phi_0}{(1+\delta)^2}\sin(2\pi t) = -\frac{Y}{1+\delta}$$

with the resulting determinant

$$\det(J) = \frac{2\pi}{1+\delta}(X^2+Y^2)\,. \tag{13}$$

Finally, we express the distribution on the screen purely in the spatial variables X and Y

$$\Psi(X,Y) = \frac{L\varphi_0}{2\pi}\frac{1}{(X^2+Y^2)^{3/2}}\,\psi\left(\frac{1}{2\pi}\arctan\left(\frac{Y}{X}\right), \frac{L\varphi_0}{\sqrt{X^2+Y^2}} - 1\right). \tag{14}$$

This equation relates the momentum distribution ψ, which originally was a function of the momentum δ and time along the pulse, to coordinates on the screen and therefore describes how the image on the screen is related to a given time dependent momentum distribution along the pulse.

We now turn to extracting the original time dependent momentum distribution ψ from an image on the screen produced by the rotating magnetic field. For this we need to invert the procedure discussed in the previous section and determine the original time-dependent momentum distribution $\psi(\tau, \delta)$ from the distribution on the image $\Psi(X, Y)$. The inverse procedure starts similarly with a two-dimensional integral

$$\psi(\tau,\delta) = \iint \Psi(X,Y)\,\delta_D\left(\tau - \frac{1}{2\pi}\arctan\left(\frac{X}{Y}\right)\right)\delta_D\left(\delta + 1 - \frac{L\varphi_0}{\sqrt{X^2+Y^2}}\right) dXdY\,. \tag{15}$$

We now need the Jacobian for the inverse system $\tilde{J}$, for which the elements are as follows

$$\begin{aligned} \frac{\partial\tau}{\partial X} &= -L\phi_0\frac{X}{(X^2+Y^2)^{3/2}} = & \frac{\partial\tau}{\partial Y} &= -L\phi_0\frac{Y}{(X^2+Y^2)^{3/2}} \\ \frac{\partial\delta}{\partial X} &= -\frac{1}{2\pi}\frac{Y}{X^2+Y^2} & -\frac{\partial\delta}{\partial Y} &= \frac{1}{2\pi}\frac{X}{X^2+Y^2}\,. \end{aligned} \tag{16}$$

With this Jacobian $\tilde{J}$, which is the inverse of J used in Equation (3), and its determinant

$$\det(\tilde{J}) = \frac{L\phi_0}{2\pi}\frac{1}{(X^2+Y^2)^{3/2}} = \frac{(1+\delta)^3}{2\pi\,(L\phi_0)^2} \tag{17}$$

we have inverted the procedure and can analyze a measurement of the screen profile through

$$\psi(\tau,\delta) = \frac{2\pi\,(L\phi_0)^2}{(1+\delta)^3}\,\Psi\left(\frac{L\phi_0\cos(2\pi\tau)}{1+\delta}, \frac{L\phi_0\sin(2\pi\tau)}{1+\delta}\right). \tag{18}$$

The momentum information is now encoded in the radial variable on the screen and the temporal information is in the angle.

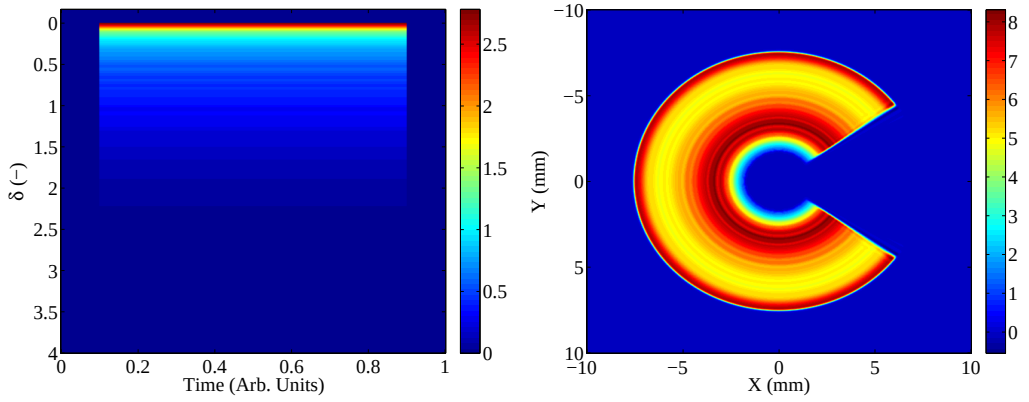

(a) Initial distribution (b) Screen image

Figure 7: The CLIC momentum distribution transformed to an image in the post-PETS diagnostic line. We have used $L = 5\,\mathrm{m}$ and $\varphi_0 = 1\,\mathrm{mrad}$. The head of the pulse, corresponding to the time $\tau = 0.1$ is in the lower right corner.

We have discussed the algorithm to extract the time-resolved momentum distribution from the proposed measurement with a rotating beam. Our goal is to perform these measurements on the decelerated CLIC drive beam, and therefore we show it in Fig. 7. The original momentum distribution shown in Fig. 7(a) is taken from Fig. 1(b), where we have let the momentum profile be constant along the bunch train. By applying Equation (14) we obtain the corresponding screen image in Fig. 7(b). Before we conclude on the performance of the method, we now look at examples of other distributions in order to evaluate the quality of the reconstruction.

4. Examples

For the evaluation of the performance we have chosen a particle distribution whose momentum along the pulse varies sinusoidally with amplitude $\delta = 0.1$. The assumed rms momentum spread Δ has the same magnitude. This momentum distribution, shown in Fig. 8(a), results in the image on the screen shown in Fig. 8(b). Here, we have neglected the effect of finite emittance. The geometric beam size on the screen is assumed to be small compared to the beam size due to the finite momentum spread. In the simulation we assume a deflection angle $\varphi_0 = 1\,\text{mrad}$ and drift length $L = 5\,\text{m}$. Using the procedure outlined above to extract the momentum distribution from the image indeed results in a distribution that is indistinguishable from the one shown in Fig. 8(a).

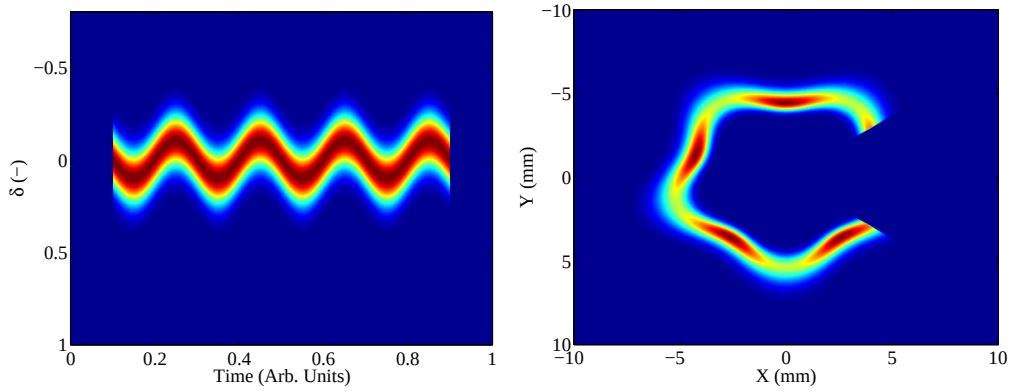

(a) Initial distribution (b) Screen image

Figure 8: Reference distribution and screen image. The momentum spread is 10% along the pulse while the average momentum oscillates with an amplitude equal to the 1σ spread.

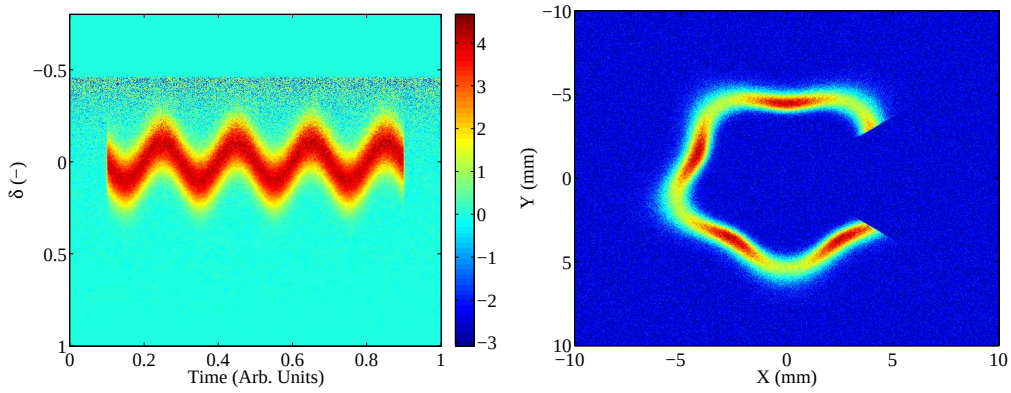

(a) Extracted distribution (b) Screen image with noise

Figure 9: Screen image and corresponding extracted momentum distribution where noise has been added. The noise is uniformly distributed around zero, with a maximum amplitude of 10% of the maximum intensity in the original image. Before inverting the image we set the pixels on the edges of the screen to zero in order to avoid a blow up near the singularity as δ approaches -1.

In order to investigate the robustness of the inversion we add random noise to the image in Fig. 8(b). The maximum noise is set to 10% of the maximum intensity in the original image and the noise is uniform in shape and centered around zero. Figure 9(b) shows the image with noise. Before extracting the momentum distribution we select the region of interest on the screen and let the pixel values on the edges be zero. This is a precaution for avoiding a strong enhancement of the noise close to the singularity as $\delta \to -1$. The singularity can be discarded since it correspond to particles at rest that will not reach the screen. Then, by extracting the distribution we obtain Fig. 9(a).

The shape and position of the snake figure remains intact, although the noise perturbs the visual impression of the distribution, especially in the low-momentum region, because the transformation between the momentum distribution and the image in Equation (14) is nonlinear and the low-momentum part is enhanced due to the denominator $(1+\delta)^3$ in Equation (18).

As already mentioned above, a finite emittance will smooth out the profile on the screen. If the geometric beam size is negligible compared to the dispersive beam size $\sigma_0 = L\varphi_0\Delta$ on the screen, the system can be inverted and the initial distribution regained by applying Eq. (18). However, if the beam size on the screen is known the screen image can be corrected through deconvolution with the geometric beam profile. This, however, requires careful use of advanced image processing and here we limit the analysis of the effect of a finite emittance to a qualitative level. In Fig. 11 we demonstrate the effect of a finite emittance by calculating the convolution of the original screen image from Fig. 8(b) with the geometric beam profile. The column to the right shows the screen images and the left column the corresponding distribution extracted from each image without taking the finite emittance into account. The geometric beam size $\sigma_{x,y}$ in the rows is given by 0.2, 1, and 2 in units of the beam width due to the momentum spread σ_0. We note that qualitative information can be extracted from the screen even for very large emittances. The general trend is that the extracted momentum spread increases with increasing emittance, while the extracted average momentum decreases.

In the CLIC decelerator the finite emittance is not expected to influence the measurement notably. Although the emittance is fairly large (150 mm mrad), the momentum spread is so large that even with a very small dispersion the geometric beam size will be negligible in comparison. In the next section we will discuss the beam size measurements, which can be used also for emittance measurements.

5. Time-resolved beam size measurements

For time-resolved beam size measurements in one plane, say horizontal, we envision to make a linear sweep in the other, here vertical, direction. Variations in the horizontal beam size along the pulse will then show up as variations of the horizontal width of the image on the screen, where time along the pulse is encoded in the vertical position. One horizontal slice of the image thus corresponds to the horizontal profile of a given temporal slice in the pulse. A large momentum spread, however, will cause vertical smearing out of particles from one temporal slice across neighboring temporal slices. In this way the large momentum spread entangles the momentum and beam size distributions. Note that this smearing out is more complex than plain convolution, because the it depends on the deflection angle and therefore varies along the pulse. Instead of solving this image processing problem, we perform simulations to investigate to what extent beam size variations can be resolved, even in the presence of large momentum spread.

We demonstrate the beam size measurement with the example in Fig. 11. A beam pulse with a variation of the horizontal beam size along the pulse is introduced. The vertical beam size is assumed to be negligible in Fig. 11 compared to the Gaussian momentum distribution, where the rms spread Δ is increased from zero to 0.15 to investigate the performance of the method. The vertical smearing of the horizontal distribution of a given temporal slice is only due to spreading of the momentum distribution, transformed according to Equation (4) to the image plane. The left column in Fig. 11 shows the images on the screen and the right column the rms beam size in the horizontal plane along the pulse, extracted from the image to the left. As the momentum spread grows, the oscillations are damped until almost no variations are visible. For every image, corresponding to a given momentum spread, we extract the standard deviation of the oscillations along the pulse and plot it in Fig. 12 as a function of momentum spread. The standard deviation decreases rapidly with increasing momentum spread and eventually approaches zero. After this point, the method does not reveal any temporal variations of the horizontal beam size. We conclude that for moderate momentum spread the method provides some qualitative information about the horizontal beam size, but is limited if the momentum spread becomes too large.

We now turn to a beam with CLIC parameters. Using only the steady-state part of the energy distribution from the histogram in Fig. 1(b), means that $\delta \in [0, 4]$. As before, we apply a linear sweep in the vertical direction and illustrate in Fig. 13 how the momentum profile is extended in the vertical direction of the screen for different deflection angles, corresponding to different points in time during the sweep. The later bunches are superimposed with the early bunches, which highlights the difficulty of extracting quantitative time information from the image.

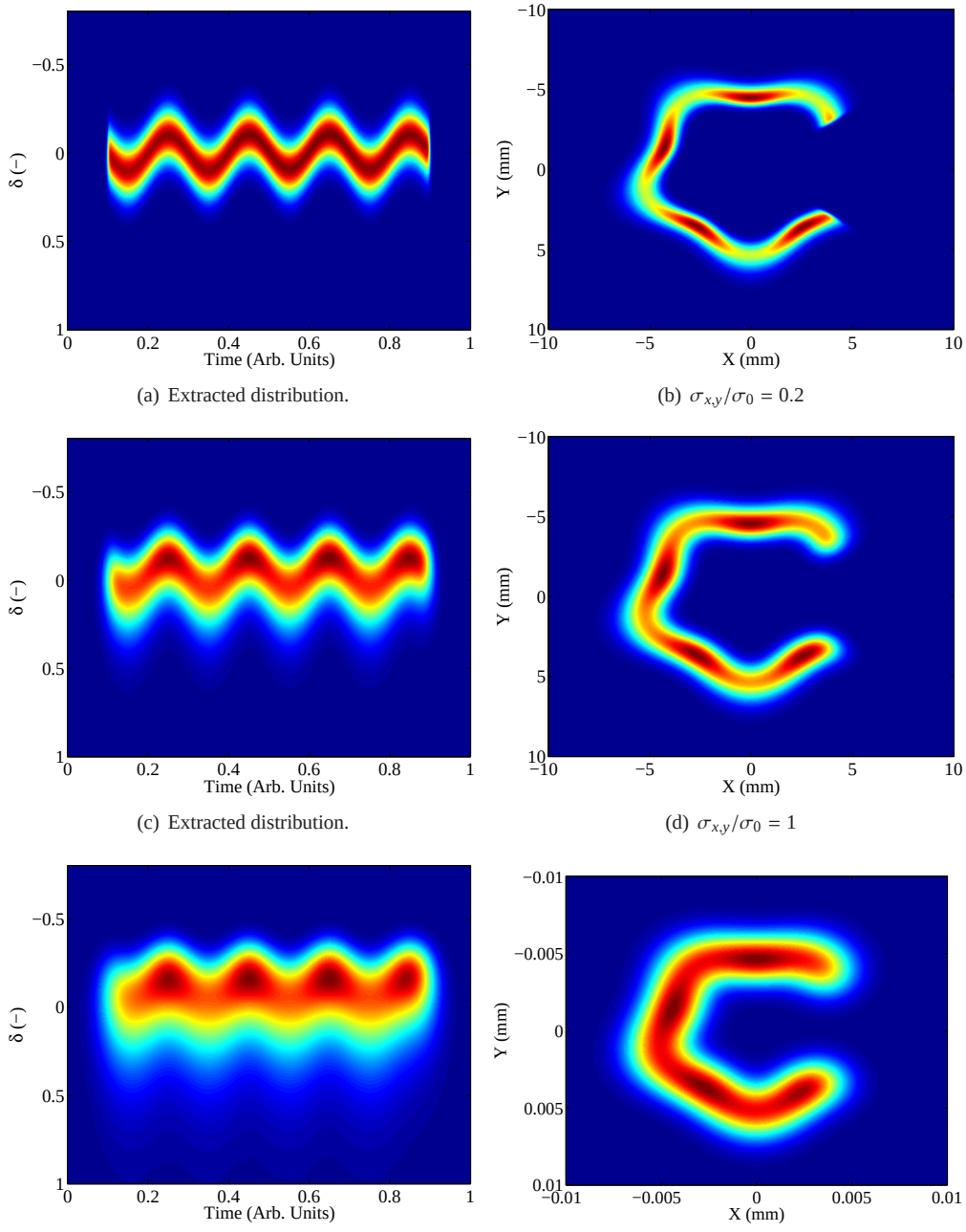

(a) Extracted distribution. (b) $\sigma_{x,y}/\sigma_0 = 0.2$

(c) Extracted distribution. (d) $\sigma_{x,y}/\sigma_0 = 1$

(e) Extracted distribution. (f) $\sigma_{x,y}/\sigma_0 = 2$

Figure 10: The extracted momentum distribution (left column) corresponding to each screen image (right column) where the geometric beam size $\sigma_{x,y}$ increases for every row compared to the dispersive beam size $\sigma_0 = L\varphi_0\Delta$. Note that the first bunch, corresponding to $\tau = 0.1$, is imaged in the lower right corner of the image in column to the right.

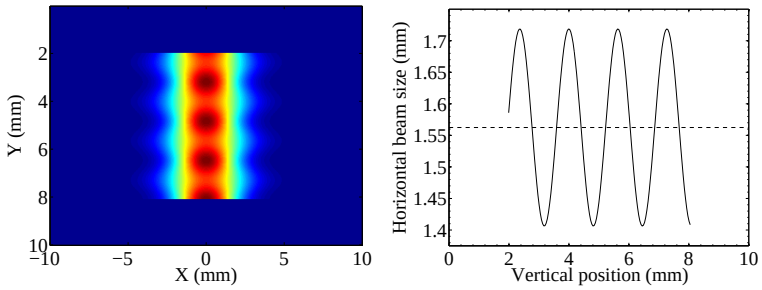

(a) Screen image for $\Delta = 0.0$. (b) Horizontal beam size

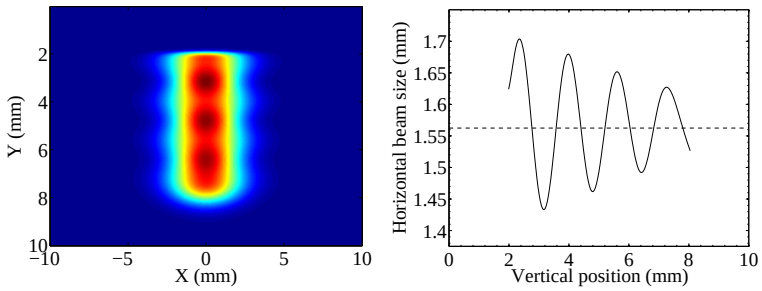

(c) Screen image for $\Delta = 0.05$. (d) Horizontal beam size

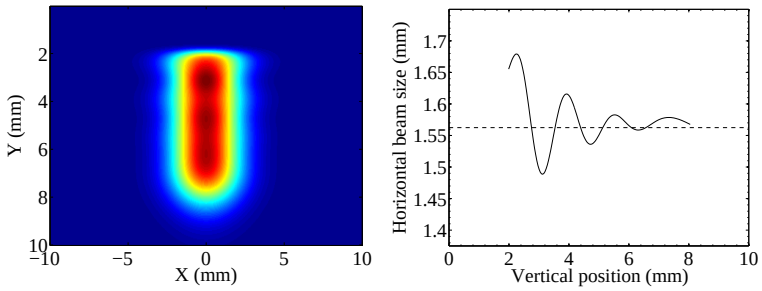

(e) Screen image for $\Delta = 0.1$. (f) Horizontal beam size

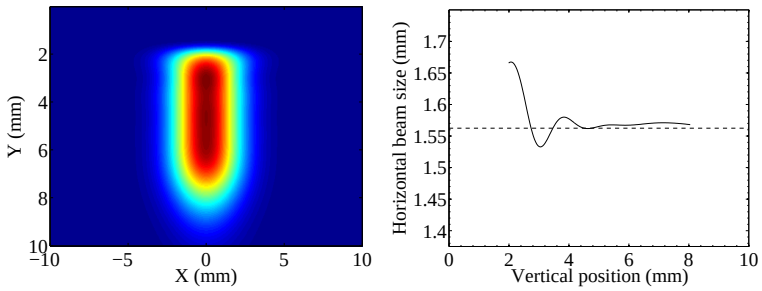

(g) Screen image for $\Delta = 0.15$. (h) Horizontal beam size

Figure 11: Images of a beam with a variation in horizontal beam width along the pulse (left column). The rms horizontal beam width along the pulse, equivalent to the vertical axis, is displayed in the right column, with the momentum spread increasing for every row. The first bunch is centered at approximately $Y = 2$ mm and the last bunch at $Y = 8$ mm.

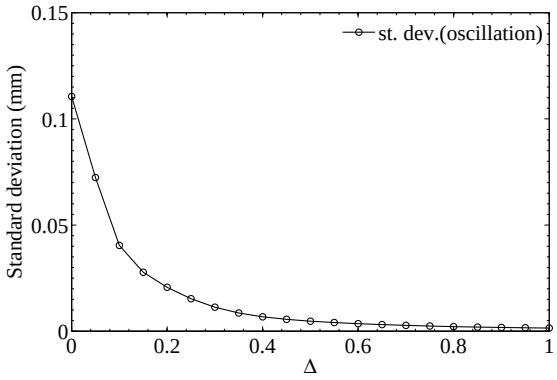

Figure 12: Standard deviation of the variation of the horizontal beam size along the pulse, as a function of the momentum spread Δ.

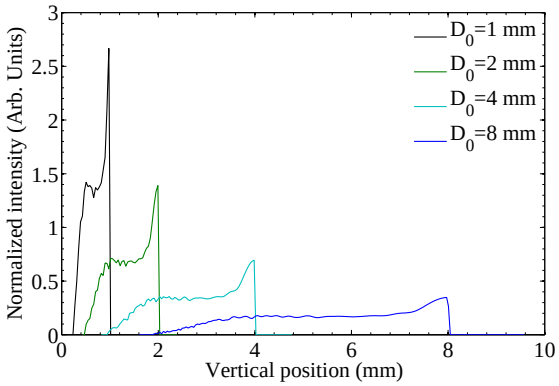

Figure 13: The CLIC momentum distribution in the vertical plane for selected deflection angles $\varphi_0 = D_0/L$. Every angle corresponds to a point in time during the sweep, where the sweep begins with a small deflection angle and ends with a large angle. The large spread leads to contamination from the late bunches of the regions where the early bunches are imaged.

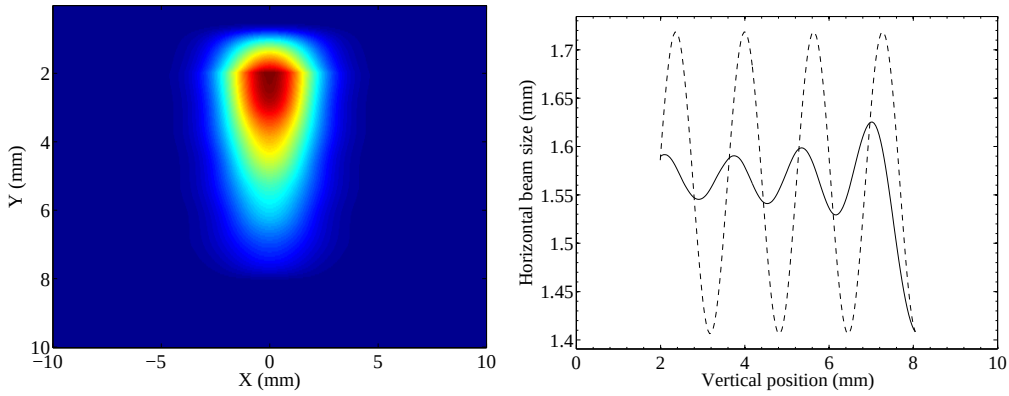

(a) Screen image for 10% variation.

(b) Horizontal beam size

Figure 14: Image of a beam with a momentum distribution corresponding to the decelerated CLIC drive beam (a). The extracted rms horizontal beam width along the pulse (b) is damped by a factor 3 on average along the train and has a phase shift of roughly 60 degrees compared to the input modulation.

Turning to the two-dimensional image, we use a Gaussian particle distribution in the horizontal direction and introduce a modulation of the horizontal beam width. We apply a linear sweep in the vertical direction and obtain a screen image from which we extract the horizontal beam width along the vertical axis. Figure 14 shows the image to the left and the extracted beam width to the right. The amplitude of the modulation is damped compared to the input by a factor 3, on average along the pulse. The vertical smearing due to the momentum spread also induces a phase shift of roughly 60 degrees. These numbers remain the same even if the amplitude of the modulation is changed.

6. Conclusions

We found that the large momentum spread of the CLIC drive beam after deceleration will lead to distorted images on a screen in a spectrometer if interpreted within a linearized model of the dispersion. We then derived the map that permits us to extract the correct momentum distribution from the screen image.

We went on to use that information to propose a method to derive the time-resolved momentum distribution along the drive beam pulse from a screen image caused by sweeping the beam in a circular pattern. It turned out that the momentum distribution can be recovered accurately as long as the geometric beam size is smaller than the beam size due to the finite momentum spread. We expect the method to become a convenient tuning tool, because the deceleration and thereby the power production can be optimized by making the circle as big as possible and the initial transient as short as possible. This should facilitate empiric tuning of the decelerator.

The beam size variation along the pulse can be extracted only in a qualitative way due to the complex smearing of the transverse profile in horizontal plane into the sweeping plane, here vertical. We expect, however, that large variations of the transverse beam sizes along the pulse are visible and permit tuning of the decelerator and preceding beam lines.

In this report we have not addressed practical issues such as the design of the kicker magnet or detailed layout of the diagnostic section. It is probably advisable to have additional kicker magnets to lead the deflected beam with its large beam power to the final beam dump in a controlled way. Neither did we discuss the deconvolution of the energy dependence of the emission of optical transition radiation from the screen which is likely to have a small effect [4]. Moreover, we expect that deconvoluting the emittance smearing from the momentum distribution can be accomplished by advanced image processing. It might also be possible to deconvolute the smearing of the beam size image due to the large momentum distribution, though this is considerably more difficult due to the variable smearing along the pulse. These points need to be addressed to establish the usefulness of the proposed diagnostic for the Post PETS line (POPEL).

Acknowledgements

We gratefully acknowledge E. Adli, Oslo University, for providing the momentum distribution at the end of the CLIC drive beam decelerator.

References

[1] S. Stapnes (Ed.), The CLIC Programme: Towards a Staged e+e- Linear Collider Exploring the Terascale, CERN-2012-005, Geneva, 2012.
[2] E. Adli, A Study of the Beam Physics in the CLIC Drive Beam Decelerator, Ph.D. thesis, University of Oslo, 2009.
[3] M. Olvegård, *et al.*, Nucl. Instr. and Meth. A, 683, 2012, pp. 29-39.
[4] M. Olvegård, *et al.*, Beam profile monitoring at the test beam line at the Compact Linear Collider test facility 3, submitted to Phys. Rev. Special Topics - Accelerators and Beams, January 2013.
[5] B. Goddard, R. Riffaud, M. Sans-Merce, W. Weterings, Conceptual Design of the LHC Beam Dumping Protection Elements TCDS and TCDQ, LHC-Project-Report-756, CERN-LHC-Project-Report-756, August 2004.
[6] D. Schulte, PLACET: a Program to Simulate Drive Beams, CERN-PS-2000-028 AE, Geneva, Switzerland, 2000.